A 10GHz CMOS RX Frontend with Spatial Cancellation of Co-channel Interferers for MIMO/Digital Beamforming Arrays

Sanket Jain, Yunqi Wang, Arun Natarajan
School of EECS, Oregon State University, Corvallis, OR

***Abstract*— An architecture for low-noise spatial cancellation of co-channel interferer (CCI) at RF in a digital beamforming (DBF)/MIMO receiver (RX) array is presented. The proposed RF cancellation can attenuate CCI prior to the ADC in a DBF/MIMO RX array while preserving a field-of-view (FoV) in each array element, enabling subsequent DSP for multi-beamforming. A novel hybrid-coupler/polyphase-filter based input coupling scheme that simplifies spatial selection of CCI and enables low-noise cancellation is described. A 4-element 10GHz prototype is implemented in 65nm CMOS that achieves >20dB spatial cancellation of CCI while adding <1.5dB output noise.**

I. Introduction

MIMO receivers (RX) are expected to play a critical role in heterogenous networks with dense spectrum reuse. Similarly, MIMO RX have also been explored for digital beamforming (DBF) phased arrays due to their flexibility and multi-beam capability [1]. In these RX, co-channel interferers (CCI) are not spatially filtered prior to the ADC and therefore the ADC must have sufficient dynamic range to accommodate both signal-of-interest (SoI) and CCI in each element which limits RX gain and wastes available ADC SNDR. Additionally, non-linearities can also degrade SNDR and create intermod/cross-mod products in the spatial frequency domain.

Analog phased arrays can reject CCI prior to ADC if CCI angle of incidence (AoI) is different from SoI but such arrays limit the RX field-of-view (FoV) and are multiple-input single-output (MISO) systems. Such analog/RF spatio-spectral filtering phased arrays have been explored in [2], [3] to reject out-of-beam (OOB) blockers. A multi-beam approach can be adopted but this requires $O(NM)$ phase shifters for M independent beams in an N-element array. However, for MIMO RX and DBF arrays, it is useful to implement spatial angle-reject RX where CCI from particular AoI are cancelled at each RX while preserving other angles in the FoV as shown in Fig. 1. This is relevant for receiving signals from all directions for subsequent DSP [4], since this approach only requires $\sim O(NP)$ phase shifters for independent rejection of P interferers.

Baseband spatial notch filtering translated to each RX element was concurrently developed in [5] using an N-path approach to achieve spatial filtering up to 1.7GHz. In this paper, we present a new architecture for RF spatial cancellation of CCI signals in each element of an N-element RX array based on the approach in Fig. 1. Measured performance from a four-element 10GHz CMOS RX frontend prototype is presented demonstrating low-noise spatial CCI cancellation.

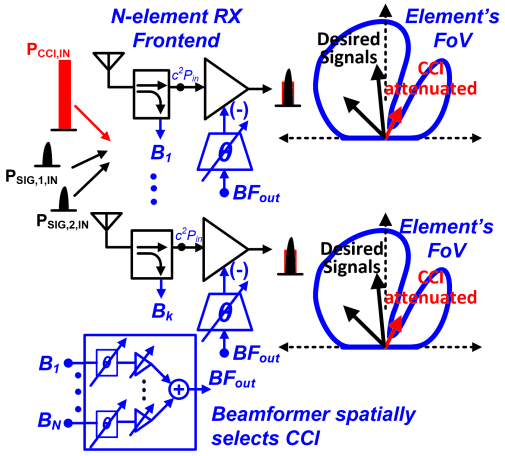

Fig. 1. MIMO/digital beamforming RX front-end with out-of-beam co-channel interference cancellation that preserves other angles in the FoV in each element for subsequent DSP.

II. Spatial CCI Cancellation

Fig. 1 represents two key circuit challenges - CCI signal estimation and low-noise cancellation.

A. Input coupling scheme:

Input signal division between the main signal path and the beamformer path in Fig. 1 as well as subsequent subtraction causes noise degradation. Assuming that cancellation path output noise is proportional to beamformer gain, there is a tradeoff in the input coupling ratio, c^2. A higher c couples a smaller signal into the beamformer, reducing loss (and hence, noise) with respect to the main signal path. However, this increases noise from the beamformer path at the cancellation node. Coupling higher power into the beamformer path (small c) is equivalent to signal loss degrading SNR.

We present an input coupling architecture which breaks this trade-off as shown in Fig. 2. Reflective terminations at coupled and thru ports in a lossless hybrid coupler ($|\Gamma_R| = 1$) lead to lossless signal transmission from the

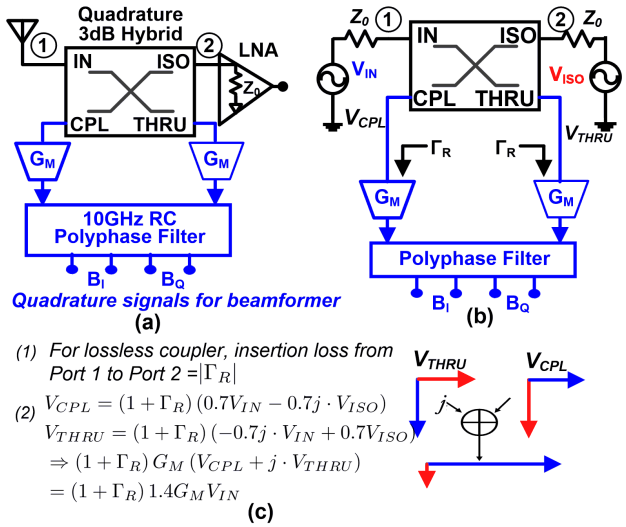

Fig. 2. Input coupling scheme based on a hybrid coupler terminated in capacitive high impedances at coupled and thru ports.

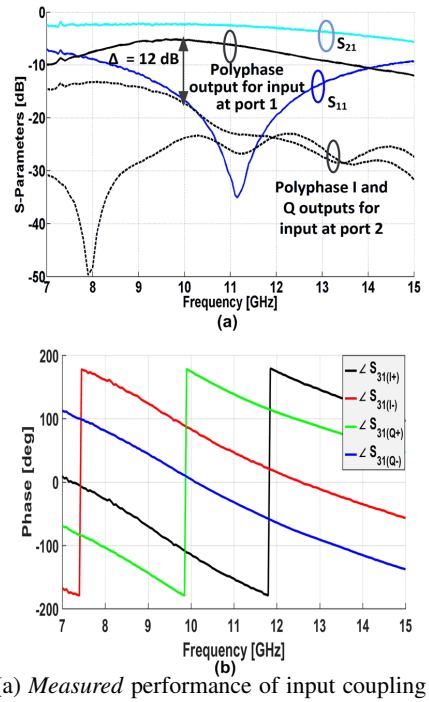

Fig. 3. (a) *Measured* performance of input coupling scheme test structure in 65nm CMOS at 10GHz for input at Port 1 and Port 2, (b) *Measured* phases of 10GHz polyphase quadrature outputs.

input port (Port 1 in Fig. 2(a)) to the isolated port (Port 2). Considering input signals at both Port 1 (V_{IN}) and Port 2, (V_{ISO}) in Fig. 2(b), for an ideal coupler, the signals at coupled and thru are in quadrature with phase lag or lead depending upon whether the input is from Port 1 or Port 2 (Fig. 2(b)). The voltage magnitude is set by reflection coefficient, Γ_R, associated with thru and coupled port terminations. Therefore, when coupled and thru ports are sensed by G_M cells (that provide high capacitive input impedance) and then combined using a polyphase filter; firstly, the combined output is proportional to the input signal (Fig. 2(c)), secondly, the loss between input and isolation ports is limited by coupler loss, and thirdly, the signal from the isolation port is rejected while the signal from the input port is amplified (Fig. 2(c)).

Notably, the coupled and thru G_M cells in Fig. 2(b) can be made low-noise and linear with size limited by frequency and input capacitance. Fig. 3(a) shows *measured* performance from a 10GHz test structure designed in 65nm CMOS. Each G_M cell consumes 6mA from 1.3V and drives a 10GHz RC polyphase. The insertion loss (limited by loss in the transformer-based lumped coupler) between Port 1 and Port 2 is around 2dB with broad input match. Fig. 3(a) also demonstrates >12dB difference in polyphase output (Fig. 2(a)) for an input at Port 1 and Port 2. The polyphase inherently generates quadrature outputs (Fig. 3(b)) that are necessary for subsequent phase shifting.

B. Cancellation beamformer:

CCI is spatially selected by the beamformer (Fig. 1). The design of the beamformer is simplified by the quadrature polyphase outputs in each element. In this work, vector-modulator based phase shifters provide variable phase and amplitude in the beamformer path for each element with 6-bit current control for each I-path and Q-path weighing cells [6]. Current summing is used to combine signals in the beamformer path. Beamformer path noise is discussed in the following section.

C. Low-noise cancellation:

The CCI that is spatially selected by the beamformer is available at its output to all elements for RF cancellation (Fig. 1). Low-noise CCI cancellation is achieved based on the noise-cancelling LNA [7]. This work builds upon the cancellation scheme proposed in [8] for full-duplex TRX while considering CCI.

Fig. 4 shows LNA schematic with CCI cancellation. The beamformer output is applied to the LNA at nodes X_k and Z_k. Noise and distortion from a signal at node X_k are inherently cancelled at noise-cancelling amplifier output [7], [8]. The anti-phase CCI signal from the beamformer at X_k cancels CCI at the LNA input and the output, Y_k. However, as shown in Fig. 4, there is a residual CCI signal at output, Z_k. Frequency-filtering can attenuate the residual signal at Z_k if it is frequency offset from SoI [8]. However, since CCI is targeted in this work, a two-point cancellation scheme is implemented where a current proportional to the CCI residual signal is injected into Z_k to cancel it. Notably, as shown in Fig. 4 due to the polyphase filtering in the coupler block (Section

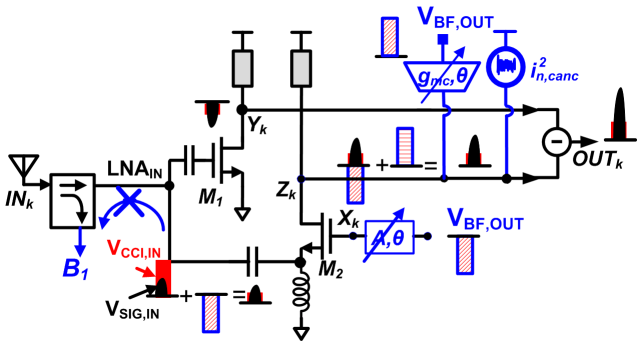

Fig. 4. Two-point CCI using noise-cancelling LNA topology: beamformer output signal with appropriate phase shift and amplitude is applied to X_k to cancel CCI and to Z_k to cancel the residual CCI signal in M_2.

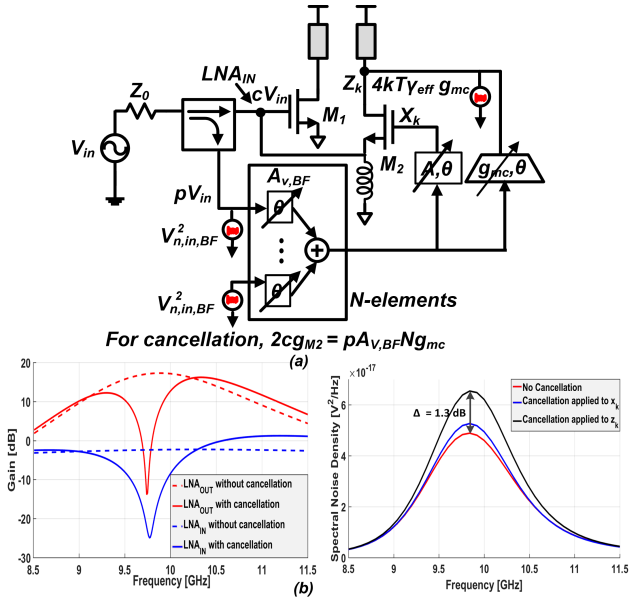

Fig. 5. (a) Simplified model for noise from cancellation, (b) Simulated gain/output noise for four-element 10GHz prototype with/without cancellation.

II-A), the impact of beamformer output feeding back into the beamformer input is reduced. While the noise due to signal at X_k is inherently cancelled; the cancellation current added to Z_k effectively increases LNA noise factor by,

$$\Delta F_{LNA,canc} = \frac{i^2_{n,canc}}{4kTR_S g^2_{M2}} = \frac{i^2_{n,canc}R_s}{4kT} \qquad (1)$$

However, the noise added by the g_{mc} cell is added to only one half of the differential pair, reducing the impact of the noise current. Based on the simplified model in Fig. 5(a), the total noise current added can be shown to be,

$$i^2_{n,canc} = \frac{4c^2 g^2_{m2} v^2_{n,in,BF}}{Np^2} + \frac{8kT\gamma_{eff}cg_{m2}}{NpA_{v,BF}} \qquad (2)$$

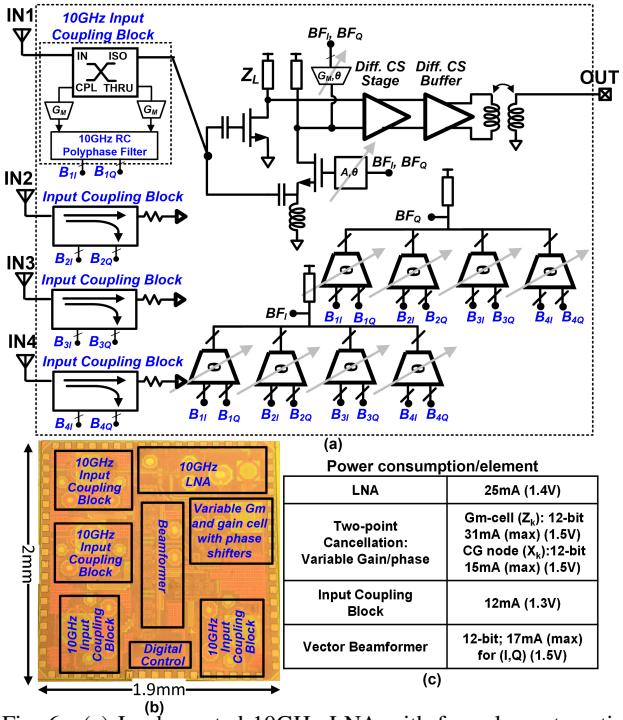

Fig. 6. (a) Implemented 10GHz LNA with four-element spatial cancellation of CCI, (b) 65nm CMOS die photo, (c) Power consumption in 10GHz RX front-end building blocks.

This shows that the firstly, $i^2_{n,canc}$ decreases with increasing N (similar to SNR improvement in phased arrays). Secondly, high $A_{v,BF}$ and p can help reduce noise. Fig. 5(b) plots simulated cancellation and output noise for a four-element 10GHz implementation which shows cancellation signal at X_k only causes marginal noise increase. Cancellation current at Z_k increases output noise by $\sim$1.3dB while providing $\sim$ 20dB cancellation.

III. 10GHz Array with Spatial Cancellation

Fig. 6 shows the implemented 4-element 10GHz prototype in 65nm CMOS. The angle reject property (shown in Fig. 1) is demonstrated in the signal path (with the LNA) for element 1. The other three elements include the input coupling scheme and vector modulators with terminations to emulate LNAs. The IC is characterized using both probe and PCB measurements and is designed assuming $\sim$1.5nH wirebond inductance for RF inputs. Fig. 7(a) shows the measured s-parameters of the signal path with cancellation inactive (probe measurements,ideal wirebond inductances). As shown in Fig. 7(b,c); when cancellation is activated, a spatial notch (>20dB) is achieved in the FoV whose location can be controlled by beamformer phase shift settings (results extrapolated from probe measurements). Fig. 7(d) demonstrates $\sim$100MHz bandwidth for 20dB cancellation.

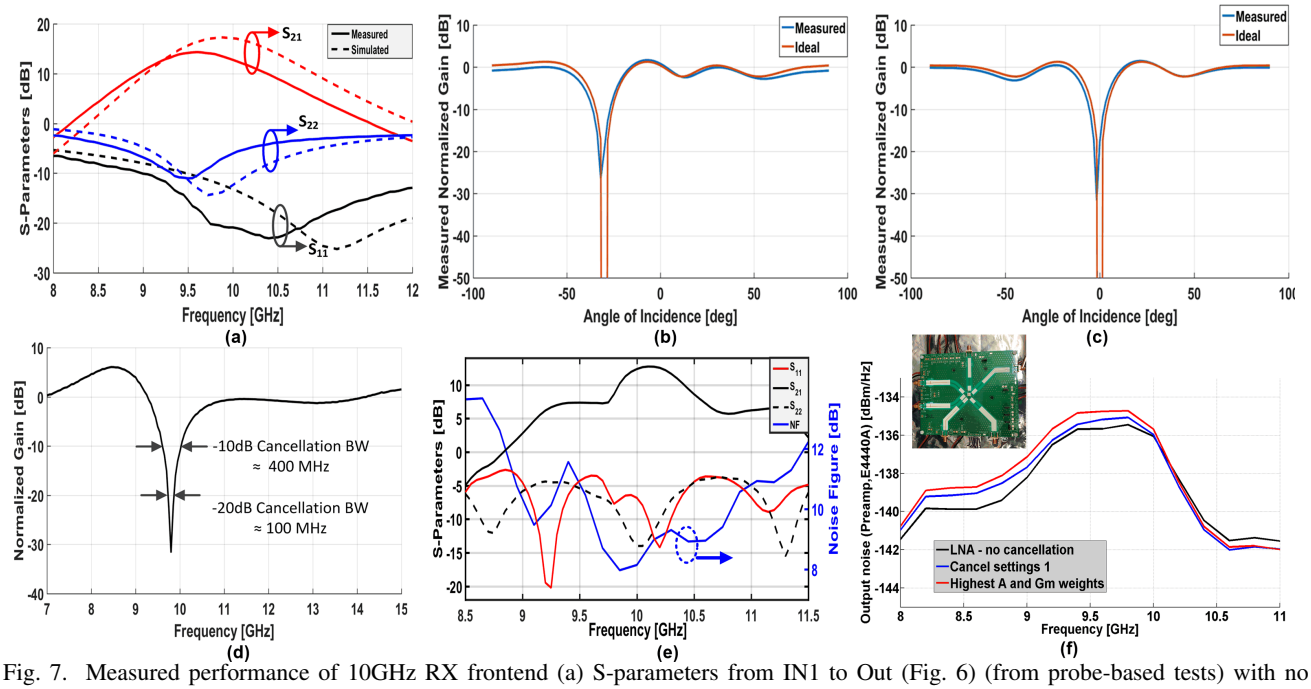

Fig. 7. Measured performance of 10GHz RX frontend (a) S-parameters from IN1 to Out (Fig. 6) (from probe-based tests) with no cancellation (b,c) Normalized gain from IN1 to Out based on probe s-parameter measurements demonstrating >20dB cancellation for input at -30°, 0° for suitable beamformer settings, (d) Measured cancellation bandwidth, (e) Measured LNA s-parameters and NF following wirebonding to PCB, (f) Measured output noise with and without cancellation.

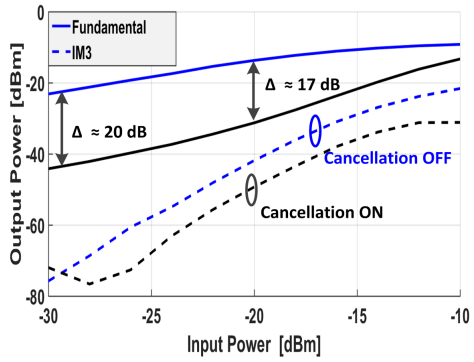

Fig. 8. Measured fundamental tones and IM3 with and without cancellation.

Fig. 7(e) shows board-level testing results - wirebond length and PCB trace coupling have degraded input matching and NF (simulations show ∼ 6.7dB NF). Output noise with and without cancellation enabled are shown in Fig. 7(f) demonstrating <1.5dB increase in output noise (measurements are ∼12dB above the noise floor of E4440A with Triquint TGA2512-SM preamp at 9.5GHz). Fig. 8 demonstrates signal cancellation on the PCB with a two-tone test - fundamental and IM3 components before and after cancellation (settings determined at low power level) are shown demonstrating lower IM3 products with cancellation even at high power levels. Future work includes extension of the proposed architecture to an RX where beamformer output is also downconverted for CCI cancellation at IF/baseband.

Acknowledgment

This work is supported by the DARPA Arrays at Commercial Timescales Program. The authors would like to thank Prof. H. Krishnaswamy, Columbia University and Dr. Roy (Troy) Ollson, DARPA for helpful discussions.

References

[1] W. Chappell and C. Fulton, "Digital Array Radar panel development," in *2010 IEEE Intl. Symp. on Phased Array Systems and Technology (ARRAY)*, Oct 2010, pp. 50–60.

[2] A. Ghaffari *et al.*, "A 4-element phased-array system with simultaneous spatial-and frequency-domain filtering at the antenna inputs," *IEEE J. Solid-State Circuits*, June 2014.

[3] S. Kalia *et al.*, "Multi-beam spatio-spectral beamforming receiver for wideband phased arrays," *IEEE TCAS I*, 2013.

[4] V. den Heuvel *et al.*, "Full MIMO spatial filtering approach for dynamic range reduction in wideband cognitive radios," *IEEE TCAS I*, Nov. 2012.

[5] L. Zhang, A. Natarajan, and H. Krishnaswamy, "A Scalable 0.1-to-1.7GHz Spatio-Spectral-Filtering 4-Element MIMO RX Array with Spatial Notch Suppression," in *2016 ISSSC*.

[6] K.-J. Koh *et al.*, "0.13-μm CMOS Phase Shifters for X-, Ku-, and K-Band Phased Arrays," *IEEE JSSC*, Nov. 2007.

[7] F. Bruccoleri *et al.*, "Wide-band CMOS low-noise amplifier exploiting thermal noise canceling," *IEEE JSSC*, 2004.

[8] J. Zhou *et al.*, "Low-noise active cancellation of TX leakage and TX noise in broadband wireless RX for FDD/Co-existence," *IEEE JSSC*, 2014.